AGU PUBLICATIONS

Geophysical Research Letters

RESEARCH LETTER
10.1002/2017GL073090

Key Points:
- Short-term variations of the double-peak pattern are inspected for the first time by means of ad hoc fixed-slit acquisitions
- A first evidence of short-term hemispheric variations is reported
- No clear correlation between Na emission and in situ IMF data was found

Correspondence to:
S. Massetti,
stefano.massetti@iaps.inaf.it

Citation:
Massetti, S., V. Mangano, A. Milillo, A. Mura, S. Orsini, and C. Plainaki (2017), Short-term observations of double-peaked Na emission from Mercury's exosphere, *Geophys. Res. Lett.*, *44*, 2970–2977, doi:10.1002/2017GL073090.

Received 14 FEB 2017
Accepted 25 MAR 2017
Accepted article online 29 MAR 2017
Published online 7 APR 2017

Short-term observations of double-peaked Na emission from Mercury's exosphere

S. Massetti[1], V. Mangano[1], A. Milillo[1], A. Mura[1], S. Orsini[1], and C. Plainaki[2]

[1]Institute for Space Astrophysics and Planetology, INAF-IAPS, Rome, Italy, [2]Italian Space Agency, ASI, Rome, Italy

Abstract We report the analysis of short-term ground-based observations of the exospheric Na emission (D1 and D2 lines) from Mercury, which was characterized by two high-latitude peaks confined near the magnetospheric cusp footprints. During a series of scheduled observations from the Télescope Héliographique pour l'Etude du Magnétisme et des Instabilités Solaires (THEMIS) telescope, achieved by scanning the whole planet, we implemented a series of extra measurements by recording the Na emission from a narrow north-south strip only, centered above the two emission peaks. Our aim was to inspect the existence of short-term variations, which were never analyzed before from ground-based observations, and their possible correlation with interplanetary magnetic field variations. Though Mercury possesses a miniature magnetosphere, characterized by fast reconnection events that develop on a timescale of few minutes, ground-based observations show that the exospheric Na emission pattern can be globally stable for a prolonged period (some days) and also exhibits fluctuations in the time range of tens of minutes.

1. Introduction

The analysis of Mercury's exosphere and its dynamics via ground-based observations of the bright sodium doublet emission (5890–96 Å) is an important way to understand the key processes lying behind the generation of the tenuous (collisionless) atmosphere of the small solar system bodies [e.g., *Potter and Morgan*, 1997; *Sprague et al.,* 1997; *Killen et al.,* 2001; *Leblanc et al.,* 2008, 2009, 2013]. The physical processes expected to play a role in the surface Na release are the following: strong bombardment by solar wind (SW) plasma driven by interplanetary magnetic field (IMF)-magnetosphere coupling, micrometeoroid impacts, and solar UV and thermal radiation, all weighted by the surface abundancies [e.g., *Milillo et al.,* 2005]. Observations of the Na exosphere exhibit very often two high-latitude peaks usually symmetrically located in both hemispheres, along the subsolar meridian, but they can also differ in intensity and/or extent. Their morphology and dynamics are conceivably associated to the direct precipitation of SW ions onto the surface (ion sputtering), driven across the magnetospheric cusps by magnetic reconnection, since none of the other known release processes is able to produce such distinctive emission pattern by itself. Recently, MErcury Surface, Space ENvironment, GEochemistry, and Ranging (MESSENGER) GRS discovered a higher Na abundance in the northern hemisphere with respect to the equatorial regions [*Weider et al.,* 2015]. However, the ion sputtering process is not expected to be able to release enough Na to account for the observed high-latitude emission peaks, due to its low efficiency. The temperature of the Na neutral population, as derived from its vertical profile (about 1200 K with a small tail at higher temperatures [*Cassidy et al.,* 2015]), fits better with a release mainly driven by the photon-stimulated desorption (PSD). By modelling the various release processes during different orbital phases, *Leblanc and Johnson* [2003] suggested that the exosphere could be described as the result of a complex relationship between surface and external environment. To account for the two-peaked Na emission, *Mura et al.* [2009] proposed that the SW ions impacting onto the surface at the cusp's footprints could loosen the Na atoms in the crystalline structure of rocks and regolith, and the subsequent desorption (induced by the actions of both temperature and photons) causes the final Na release into the exosphere. *Sarantos et al.* [2009] suggested that ion impacts induce enhanced diffusion in the regolith grains bringing more Na onto the upper surface layer. *Potter et al.* [2006] statistical analysis based on 1997–2003 data reported that about one third of the observations show north/south asymmetries, randomly distributed in True Anomaly Angle (TAA) and longitudes, and they concluded that such asymmetries seem then to be related to an external cause, possibly linked to the IMF configuration. *Mangano et al.* [2015] performed a statistical analysis based on a 5 years data set (2009–2013) of Na exospheric observations. The Na emission was categorized into eight different patterns, and their occurrence was investigated, as well as their correlation with in situ IMF data. The study shows that the double-peak patterns are the most common Na

exospheric features (61%) and that they often persist for several hours, or even days, supporting the idea that quasi-steady SW ion precipitation through the polar cusps plays a key role in their generation.

Up to date, the ground-based observation campaigns of the Mercury's sodium exosphere have been typically performed by recording the emission from whole planet, on per-hour basis or longer. While suitable for the study of the global morphology and its midterm to long-term variability, this time resolution does not allow to inspect possible shorter-term variability on timescales comparable with the Mercury's magnetospheric phenomena (few minutes) and/or with the exospheric response time, which is of the order of ballistic time of the released Na atoms (tens of minutes). To overcome this limitation, we performed a short series of ad hoc observations by recording over time (1 h) the Na emission coming from just a narrow latitudinal strip crossing both the northern and southern cusps. These "fixed-slit" observations were taken in between the planned full disk scans, during the June 2012 observational campaign we carried out at THEMIS. The main intent of this work is to inspect potential short-time variations in the Na exospheric emission and to check for possible correlations with in situ IMF data from MESSENGER. For the first time, thanks to this unique set of simultaneous observations from ground and space, we can show and analyze the short-term variations of the double-peak feature of the Na exosphere of Mercury.

2. THEMIS Na Data

Data of the Na exosphere of Mercury are obtained by means of the THEMIS solar telescope (Tenerife, Canary Islands, Spain) [*López-Ariste et al.,* 2000]. THEMIS is equipped with a 0.9 m primary mirror with 15.04 m focal length that, thanks to its optical design, is characterized by a low level of scattered light. Because of this capability, it can be used during the daylight to image the Na exosphere of Mercury with a high contrast (with respect to sky brightness), for several hours per day. A long campaign of observations has been performed since 2007, and a wide database is now available, leading to a number of studies [e.g., *Leblanc et al.,* 2008, 2009, 2013; *Leblanc and Johnson*, 2010; *Mangano et al.,* 2013, 2015]. Since 2009, THEMIS was used together with the MulTi Raies (MTR) spectrograph in multiline mode, with two cameras recording the Na D1 and D2 lines at the same time. The spectral dispersion was of 11 mÅ per pixel and the spectral resolution 27 mÅ, about 220,000 resolving power. THEMIS is equipped with a tip-tilt mirror and an image stabilizer optical system, which actively contribute to reduce noise due to both atmospheric seeing fluctuations and telescope vibrations (further details can be found in the above mentioned references).

The standard (full-disc) Na images taken at THEMIS require about 1 h to be completed: to reduce the signal-to-noise ratio, every data acquisition is built by 10 scans with 2 s of integration, and every north-south strip of pixels is obtained by averaging 10 consecutive acquisitions, resulting in a total of 200 s integration time. The spectrograph slit is then shifted in the east-west direction by an amount equal to the slit width (1.27 cm.) to obtain the next strip of pixels. Every full-disc image is made up by about 18 contiguous north-south scans, resulting in 18×200 s = 3600 s of observation time.

Studies based on the analysis of full-disc images cannot inspect variations in the exospheric Na emission on a timescale shorter than the acquisition time (1 h). To overcome this constraint, we achieved a series of extra measurements by keeping the spectrograph's slit position fixed across the two Na peaks and then by recording the emission coming from this narrow region only (Figure 1). As for the standard full-disc images, 18 consecutive scans of 200 s each were recorded. The tip-tilt correction ensures that the slit position is preserved during all the exposure time. The full-disc images recorded before and after each fixed-slit image are used also to validate the intensity observed during the fixed-slit measurements and to estimate the seeing value. When possible, the extra fixed-slit images were recorded when the MESSENGER spacecraft was outside the Mercury's magnetosphere, in the upstream SW, in order to have unperturbed IMF data. The present data set consists in 29 images (21 full disc +8 fixed slit) recorded during 7–9 June 2012. The relative size of Mercury was between 5.4 in. and 5.6 in., the disc visibility 86%–84%, and the TAA was 55.2°–68.2°.

3. Analysis and Discussion

Figure 2 shows the sequences of both "standard" and "fixed-slit" images, during 7 June (top), 8 June (middle), and 9 June (bottom): the 1 min data and the 1 h averages of the three IMF components and its module are plotted for each day (B_X, B_Y, B_Z, and $|B|$). The black arrow under each image approximately indicates its acquisition time length. The gray dashed areas mask the periods when the spacecraft was inside the

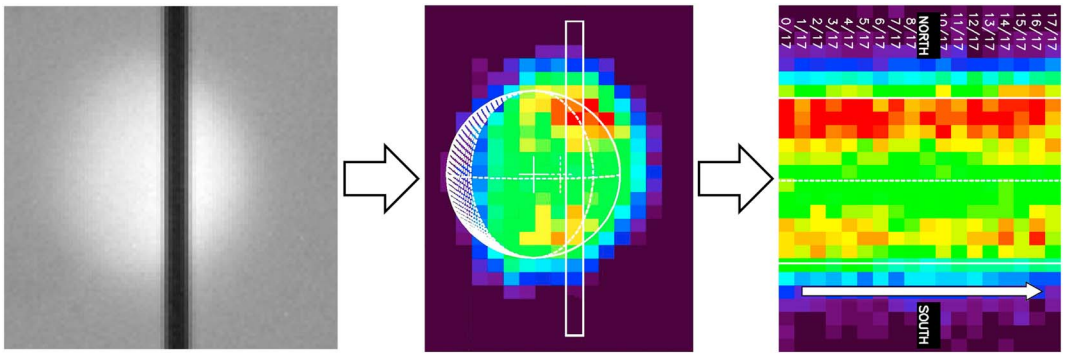

Figure 1. Sketch of a fixed-slit acquisition. (left) Visible light image showing the spectrograph's slit perpendicular to the planet's equator, at about one fourth of the disc size (only the lightened portion is visible), in the sunward direction. (middle) Spectrograph slit crossing the cusp areas on a full-disc Na image. (right) Resulting sequence of 18 consecutive fixed-slit acquisitions plotted side by side: The horizontal white lines mark the northern and southern planet's edges, which are close to the true north and south poles, and the equator position (dashed).

magnetosphere, and then no IMF data are available. The red-colored areas emphasize the IMF $B_Z < 0$ intervals, a condition that on Earth is an indicator of the (geo)effectiveness of an interplanetary perturbation impinging on the magnetosphere.

Data in Figure 2 clearly show the distinctive double-peaked Na emission on the dayside high-latitude regions, which is the recurrent pattern most observed in Mercury's exosphere [*Killen et al.,* 2001; *Leblanc et al.,* 2008, 2009; *Mangano et al.,* 2015]. *Mangano et al.* [2015] identified four different types of double-peak patterns, namely, two nearly symmetrical peaks (2P), two peaks with the northern/southern more intense (2PN and 2PS, respectively), and two peaks connected (2PC) by a narrow band along the limb, which often coincides with the subsolar meridian. In the present case, the Na emission varied between the 2P and the 2PN patterns, with the northern hemisphere generally dominating.

A persistent double peak was observed lasting for more than three consecutive days (it was present also on 6 June). This pattern is likely to be linked to ion precipitation, and we can then assert that in spite of the short timescale of the Mercurian magnetosphere and its fast response to the IMF/SW variations, a continuous precipitation of plasma through the magnetospheric cusps must exist [e.g., *Varela et al.* [2016]]. This condition is well known to take place in the Earth's magnetosphere, thanks, for example, to the observation of a stable UV proton auroral emission from space [*Frey et al.,* 2002], induced by the direct precipitation of SW ions into the cusps, driven by a quasi-steady magnetic reconnection regime.

In this context, the fact that the Na emission from the southern cusp region is generally weaker than the northern one is rather puzzling: data from MESSENGER fit well with a magnetic dipole displaced northward by about 0.2 R_M, and the southern cusp is therefore expected to be about 4 times wider than the northern one [*Anderson et al.,* 2011]. Consequently, a significant fraction of the dayside southern hemisphere should be directly exposed to SW ion impacts [e.g., *Winslow et al.* [2014]] and a broader and/or more intense Na exospheric emission should be observed. Conversely, a double-peak pattern dominated by the southern emission is a feature rarely observed from ground-based surveys, as is apparent from the analysis of the whole data set collected from THEMIS telescope recorded between 2009 and 2013 [see *Mangano et al.,* 2015, Table 1]. As H^+ ions were observed to be injected toward the cusp(s) via magnetic merging at dayside magnetopause [*Raines et al.,* 2014], a deficit in the related Na emission could be due to the fact that part of these ions actually does not reach the surface or does not have enough energy to promote the sodium release from the soil. Local shielding caused by higher-order magnetic field components [e.g., *Christensen* [2006]; *Richer et al.* [2012]], or by the induction effect driven by a conductive core [e.g., *Jia et al.* [2015]], may be possible explanations. Alternatively, because of the weaker magnetic field, the sodium content in the soil of the southern hemisphere could have been more depleted than the northern one, or long-term micrometeoritic impact asymmetries could have led to uneven Na refurbishment in the upper layers of the soil in the two hemispheres.

In order to inspect possible signatures caused by IMF variations, Figure 2 displays the values of the three components of the IMF and its module. The period under investigation was characterized by a stable IMF

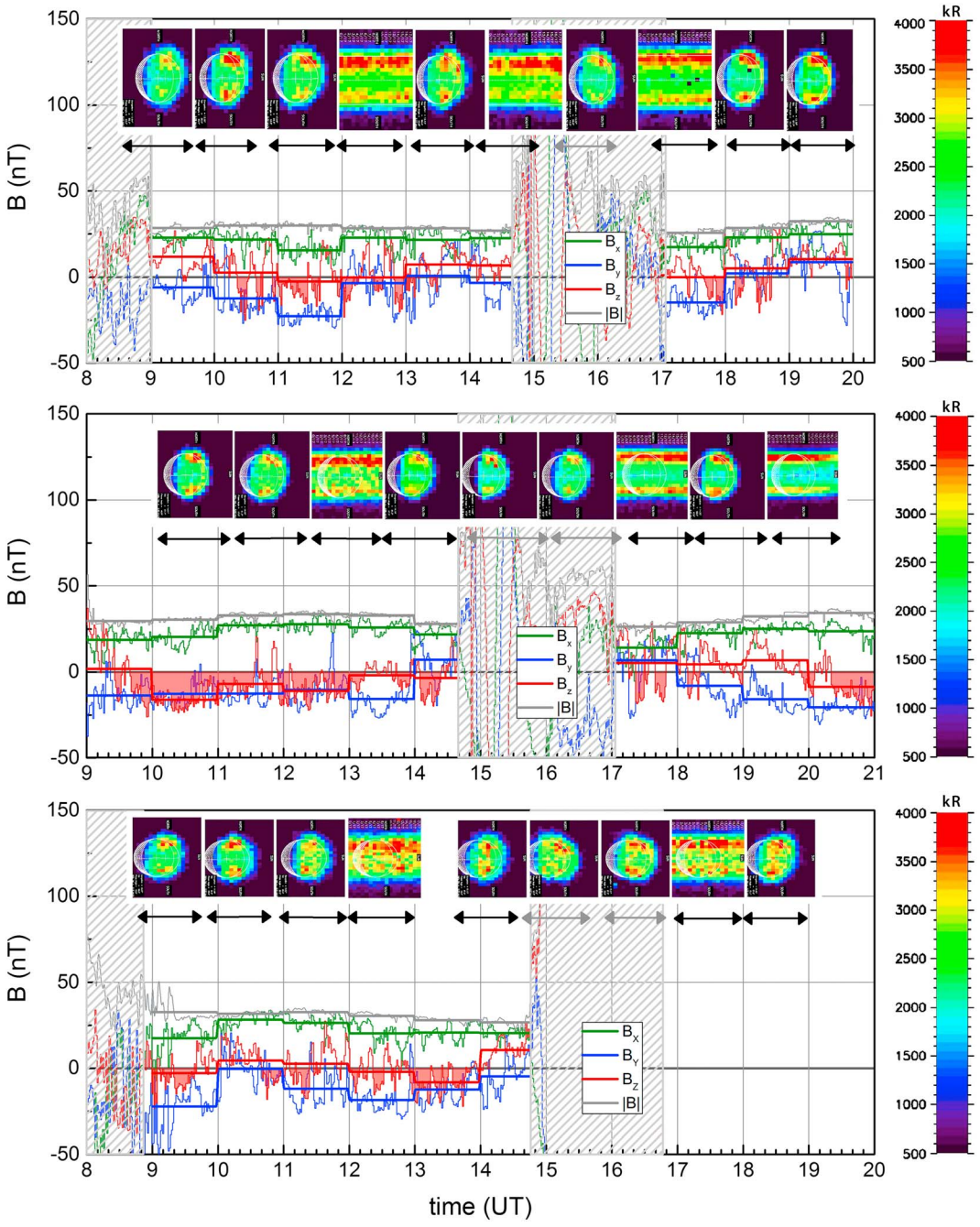

Figure 2. Standard and fixed-slit images, during (top) 7 June, (middle) 8 June, and (bottom) 9 June 2012. The black arrows approximately indicate the acquisition time of each image. In the lower part of each panel, the plots of the IMF values are shown (B_X, B_Y, B_Z, and $|B|$; see legend). The 1 h averages are superposed to the 1 min plots (same colors) of each IMF components. The dashed areas mask the periods when the spacecraft was inside the Mercurian magnetosphere and no in situ IMF data are available. The red-colored area mark the periods when the IMF B_Z component is negative, a condition that in the Earth's case is known to be an indicator of the (geo)effectiveness of an upstream perturbations. No MAG data are unavailable after 15:00 of 9 June 2012 (Figure 2, bottom).

$B_X \approx 25$ nT and a negative IMF B_Y for most of the time, accordingly with an IMF directed sunward, approximately along the nominal Parker's spiral direction. As expected, the B_Z was the most variable IMF component, showing frequent oscillations between positive and negative values. The only prolonged B_Z negative period occurred in the first half of 8 June (~9:30–13:15 UT, Figure 2, middle) and lasted for about 4 h; it does not seem to cause any noticeable effect on the observed Na pattern, which persisted on a

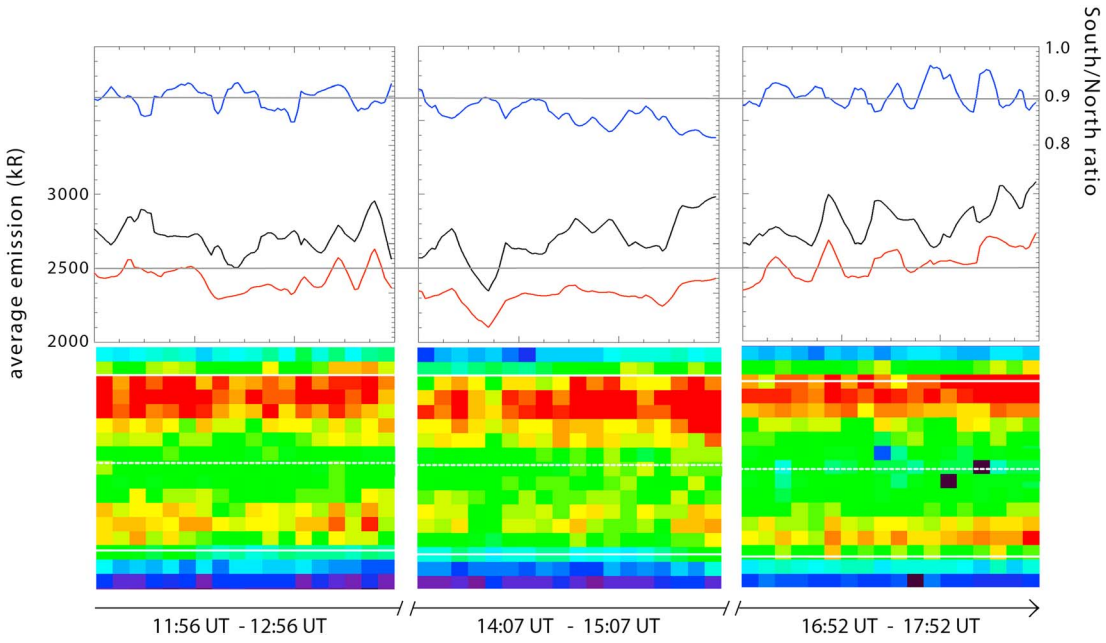

Figure 3. Time evolution of the Na exospheric emission from the Mercurian cusps during 7 June 2012, recorded between about 12 UT and 18 UT (see Figure 2, top). The average Na emission from the northern hemisphere (black line), the southern hemisphere (red line), and their ratio (blue line) is plotted on the top of each image. Two horizontal gray lines give a reference to evaluate the trends: The one on the top indicates the average value of the south/north ratio in the first image, and the second one is set to 2500 kR. The southern cusp emission clearly dimmed between about 14 UT and 15 UT (Figure 3 middle column).

double-peak pattern dominated by the northern hemisphere. No clear signatures of a correlation between IMF components and the Na exospheric emission on the midterm or short term can be detected during the whole period under analysis, in both full-disc and fixed-slit images.

From a statistical point of view, the double-peak 2P and 2PN patterns were found to be mainly associated to negative IMF B_Z periods (60%) and positive IMF B_X periods (78%) [*Mangano et al.,* 2015]. From the same analysis, double-peak patterns 2P and 2PN resulted also to be more frequent (73%) when the IMF is high (IMF $|B| > 25$ nT). The fact that in the present study the double-peak pattern appears to be almost constant, irrespective to the IMF B_Z direction and strength, could be explained in terms of magnetic reconnection rate. By taking in consideration the mean values of both SW speed and density at the orbit of Mercury [e.g., *Sarantos et al.* [2007]], a value of IMF $|B| > 25$ nT is likely to be associated to a low (<5) upstream Alfvénic Mach number ($M_A = \frac{\sqrt{n}}{20} V/|B|$), which—by inducing a low plasma β in the magnetosheath—has been reported to drive higher reconnection rate at Mercury, almost regardless of the IMF orientation [*DiBraccio et al.,* 2013; *Slavin et al.,* 2014]. During the whole time period here analyzed the module of IMF was actually greater than 25 nT, and this could be a realistic explanation for the lack of correlation with the observed Na emission. From Figure 2 we can also note the absence of any north-south asymmetry induced by the IMF B_x sign. Such an asymmetry, as described in several works [e.g., *Sarantos et al.,* 2001; *Kallio and Janhunen,* 2003; *Massetti et al.,* 2007], should take place since a positive/negative IMF B_x is believed to favor the high-latitude reconnection in the southern/northern hemisphere. A constant IMF $B_x > 0$, as in the present case, should then boost the already wider Mercury's southern cusp, which is the opposite of what we observe. The effect should be stronger as the low-latitude reconnection weakens, that is, for high Alfvénic Mach number and IMF $B_z > 0$ [*DiBraccio et al.,* 2013; *Slavin et al.,* 2014].

The first sequence (Figure 2, top) is the most clean and interesting one, and the corresponding fixed-slit images are shown in more detail in Figure 3. The average Na emission intensities from the northern and southern hemispheres, and their ratio (S/N), are shown on the top of each image. A threshold of 2200 kR was used to extract the more intense Na cusp emission from the background.

It can be noticed that the mean north and south intensities undergo several short-term variations occurring nearly in phase on both hemispheres. Because of the lack of complementary SW speed and density data, it is difficult to understand if these in-phase variations are (a) associated to a real global Na emission variability

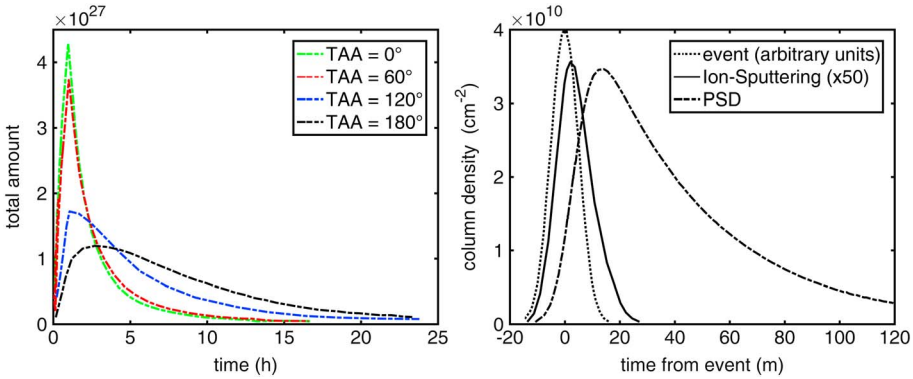

Figure 4. (left) Simulated 3-D total amount of sodium in the global exosphere versus time, after being injected during the first hour (total flux = 2.5×10^{28}), computed for four different values of TAA. (right) Simulated 2-D column Na density versus time for both ion sputtering (solid line) and PSD (dashed line), computed for a prompt event occurring at $t = 0$ (dotted line).

(related to changes in the ion precipitation flux into the cusps), (b) caused by local phenomena, as fluctuations of the atmospheric transparency, or (c) due to a combination of both effects, since they are not exactly symmetrical in both hemispheres.

However, it must be stressed that such short-term Na variations are unlikely to be produced by the atmospheric seeing only, because of the THEMIS image stabilizer optical system that actively contributes to eliminate most of the fluctuation caused by the seeing itself (up to about 90%). Moreover, to minimize potential seeing effects, every north-south scan is built up by averaging 10 consecutive data acquisitions, for a total of 200 s integration time. This time interval is greater than the timescale of the reconnection-driven circulation at Mercury, which is about 1–3 min [e.g., *Slavin et al.,* 2010]. To filter away the in-phase variations and eliminate any bias that could be introduced by atmospheric perturbations, we can look at the relative variations between the northern and southern sodium signals. The computed south/north mean emission ratio is shown in Figure 3 (top row, blue lines): while the Na emission remains nearly constant in the first image (left), the difference between southern emission and northern emission increases and the south/north ratio decreases between 14:07 UT and 15:07 UT (middle). The south/north ratio then recovers in the last image (right), and after 17:00 UT both intensities increase. We believe that Figure 3 displays a real change of the Na exospheric emission, with a timescale of the order of about 1 h, which is comparable with the photoionization Na lifetime at Mercury (estimated to be ≈1.5 ÷ 3.0 h, but the actual value is still controversial) [see *Killen et al.,* 1999; *Combi et al.,* 1997]. In this context, it must be also noted that the timescale of the Na emission variations in the exosphere of Mercury is strongly related with the TAA due to both radiation pressure and photoionization [*Mura*, 2012]. In Figure 4 (left), we show a numerical simulation of the temporal variability of the total content of Na in the exosphere of Mercury: Na atoms are "injected" in the environment for the first hour, and then their decay is derived for TAA = 0°, 60°, 120°, and 180° [*Mura*, 2012]. TAA values in the present data set range between 55° and 68° and then can be described by the TAA = 60° simulated case (dashed red line, Figure 4, left), which implicates the shortest time response, with a decrease of more than $1/e$ after about 2 h.

Faster variations on a timescale of roughly 10 min are observed too, but it is difficult to understand if they are real changes in the exospheric Na emission or modulations caused by other effects (e.g., by the Earth's atmosphere). However, we find that the timescale of these short-term variations is consistent with the decay timescale of localized Na "injection," e.g., at the cusp footprint, as it results by applying a simplified two-dimensional version of the *Mura* [2012] model, for both ion sputtering and PSD (Figure 4, right).

4. Conclusions

We reported and analyzed a steady double-peaked Na exospheric emission at Mercury's cusps that was observed to persist for more than three consecutive days (7–9 June 2012).

The southern Na emission was always narrower and weaker that the northern one, a fact which seems to conflict with the magnetic field model based on new data from MESSENGER [*Anderson et al.,* 2011],

implying a wider southern cusp area. Given that the observed high-latitude Na emission is believed to be linked to the SW entry through the cusps, then a broader signal should be frequently observed from the southern hemisphere.

The lack of any significant one-to-one relationship between the observed Na exospheric emission intensity/morphology and the in situ IMF data matches the results of recent works that show that a low upstream Alfvénic Mach number—resulting in a low plasma β in the magnetosheath—can drive high reconnection rate at Mercury, nearly irrespective of the IMF direction [*DiBraccio et al.,* 2013; *Slavin et al.,* 2014].

A set of complementary fixed-slit observations shows that the Na exospheric emission from both the northern and southern hemispheres undergoes a series of in-phase intensity oscillations on a timescale of 10–15 min.

On the base of the available data it is not possible to understand if these oscillations are real Na emission variations induced by SW perturbations or just artifacts caused by atmospheric fluctuations (e.g., changes in transparency). However, by means of a simple numerical model, we show that such short-term variations, in the range 10–15 min, are compatible with the response time of the Na exospheric release, as induced by impulsive events (likely caused by ion precipitation).

Finally, by comparing the three fixed-slit images recorded on the first day (7 June), we detected a longer-term variation in the south/north emission ratio, on a timescale of about 1 h, which definitely seems decoupled by local atmospheric fluctuations. This 1 h variation is compatible with the Na photoionization lifetime and the fastest decay lifetime of simulated global Na exosphere, which takes place at small TAAs (≈0°–60°), as in the present observations.

Acknowledgments
Ground-based observation campaign of Mercury's Na exosphere from THEMIS was started and organized by F. Leblanc; the INAF participation is led by V. Mangano. Data are available online at "http://themis.iaps.inaf.it." The authors thank the THEMIS staff in Tenerife (Canary Islands, Spain) for their fruitful help during the observation campaigns. This work was supported by the ASI-SERENA contract I/081/09/0 "SERENA: scientific activity." MESSENGER MAG data used in this study are available from the NASA Planetary Data System (MESS-E/V/H/SW-MAG-3-CDR-CALIBRATED-V1.0).

References

Anderson, B. J., C. L. Johnson, H. Korth, M. E. Purucker, R. M. Winslow, J. A. Slavin, S. C. Solomon, R. L. McNutt Jr., J. M. Raines, and T. H. Zurbuchen (2011), The global magnetic field of Mercury from MESSENGER orbital observations, *Science*, *333*, 1859–1862, doi:10.1016/j.pss.2011.01.010.

Cassidy, T. A., A. W. Merkel, M. H. Burger, M. Sarantos, R. M. Killen, W. E. McClintock, and R. J. Vervack, Jr. (2015), Mercury's seasonal sodium exosphere: MESSENGER orbital observations, *Icarus*, *248*, 547–559, doi:10.1016/j.icarus.2014.10.037.

Combi, M. R., M. A. DiSanti, and U. Fink (1997), The Spatial distribution of gaseous atomic sodium in the Comae of comets: Evidence for direct nucleus and extended plasma sources, *Icarus*, *130*, 336–354.

Christensen, U. R. (2006): A deep dynamo generating Mercury's magnetic field, *Nature*, *444*, 1056–1058, doi:10.1038/nature05342.

DiBraccio, G. A., J. A. Slavin, S. A. Boardsen, B. J. Anderson, H. Korth, T. H. Zurbuchen, J. M. Raines, D. N. Baker, R. L. McNutt Jr., and S. C. Solomon (2013), MESSENGER observations of magnetopause structure and dynamics at Mercury, *J. Geophys. Res. Space Physics*, *118*, 997–1008, doi:10.1002/jgra.50123.

Frey, H. U., S. B. Mende, T. J. Immel, S. A. Fuselier, E. S. Claflin, J.-C. Gérard, and B. Hubert (2002), Proton aurora in the cusp, *J. Geophys. Res.*, *107*(A7), 1091, doi:10.1029/2001JA900161.

Jia, X., J. A. Slavin, T. I. Gombosi, L. Daldorff, G. Toth, B. van de Holst (2015), Global MHD simulations of Mercury's magnetosphere with coupled planetary interior: Induction effect of the planetary conducting core on the global interaction, *J. Geophys. Res. Space Physics*, *120*, 4763–4775, doi:10.1002/2015JA021143.

Kallio, E., P. Janhunen (2003), Solar wind and magnetospheric ion impact on Mercury's surface, *Geophys. Res. Lett.*, *30*(17), 1877, doi:10.1029/2003GL017842.

Killen, R. M., A. Potter, A. Fitzsimmons, and T. H. Morgan (1999), Sodium D2 line profiles: Clues to the temperature structure of Mercury's exosphere, *Planet. Space Sci.*, *47*, 1449–1458, doi:10.1016/S0032-0633(99)00071-9.

Killen, R. M., A. E. Potter, P. Reiff, M. Sarantos, B. V. Jackson, P. Hick, and B. Giles (2001), Evidence of space weather at Mercury, *J. Geophys. Res.*, *106*, 20,509–20,525, doi:10.1029/2000JE001401.

Leblanc, F., A. Doressoundiram, N. Schneider, V. Mangano, A. López Ariste, C. Lemen, B. Gelly, C. Barbieri, and G. Cremonese (2008), High latitude peaks in Mercury's sodium exosphere: Spectral signature using THEMIS solar telescope, *Geophys. Res. Lett.*, *35*, L18204, doi:10.1029/2008GL035322.

Leblanc, F., A. Doressoundiram, N. Schneider, S. Massetti, M. Wedlund, A. López Ariste, C. Barbieri, V. Mangano, and G. Cremonese (2009), Short-term variations of Mercury's Na exosphere observed with very high spectral resolution, *Geophys. Res. Lett.*, *36*, L07201, doi:10.1029/2009GL038089.

Leblanc, F., and R. E. Johnson (2003), Mercury's sodium exosphere, *Icarus*, *164*, 261–281, doi:10.1016/S0019-1035(03)00147-7.

Leblanc, F., and R. E. Johnson (2010), Mercury exosphere: I. Global circulation model of its sodium component, *Icarus*, *209*, 2, 280–300, doi:10.1016/j.icarus.2010.04.020.

Leblanc, F., J.-Y. Chaufray, A. Doressoundiram, J.-J. Berthelier, V. Mangano, A. López-Ariste, and P. Borin (2013), Mercury exosphere: III. Energetic characterization of its sodium component, *Icarus*, *223*, 963–974, doi:10.1016/j.icarus.2012.08.025.

López-Ariste, A., J. Rayrole, and M. Semel (2000), First results from THEMIS spectropolarimetric mode, *Astron. Astrophys. Suppl. Ser.*, *142*, 137–148, doi:10.1051/aas:2000144.

Mangano, V., S. Massetti, A. Milillo, A. Mura, S. Orsini, and F. Leblanc (2013), Dynamical evolution of sodium anisotropies in the exosphere of Mercury, *Planet. Space Sci.*, *82-83*, 1–10, doi:10.1016/j.pss.2013.03.002.

Mangano, V., S. Massetti, A. Milillo, C. Plainaki, S. Orsini, R. Rispoli, and F. Leblanc (2015), THEMIS Na exosphere observations of Mercury and their correlation with in-situ magnetic field measurements by MESSENGER, *Planet. Space Sci.*, *115*, 102–109, doi:10.1016/j.pss.2015.04.001.

Massetti, S., S. Orsini, A. Milillo and A. Mura (2007), Modelling Mercury's magnetosphere and plasma entry through the dayside magnetosphere, *Planet. Space Sci.*, *55*, 1557–1568, doi:10.1016/j.pss.2006.12.008.

Milillo, A., et al. (2005), Surface-exosphere-magnetosphere system of Mercury, *Space Sci. Rev.*, *117*, 397–443, doi:10.1007/s11214-005-3593-z.
Mura, A., P. Wurz, H. I. M. Lichtenegger, H. Schleicher, H. Lammer, D. Delcourt, A. Milillo, S. Orsini, S. Massetti, and M. L. Khodachenko (2009), The sodium exosphere of Mercury: Comparison between observations during Mercury's transit and model results, *Icarus*, *200*, 1–11, doi:10.1016/j.icarus.2008.11.014.
Mura, A., (2012), Loss rates and time scales for sodium at Mercury, *Planet. Space Sci.*, *63-64*, 2–7, doi:10.1016/j.pss.2011.08.012.
Potter, A. E., and T. H. Morgan (1997), Sodium and potassium atmospheres of Mercury, *Planet. Space Sci.*, *45*, 95–100, doi:10.1016/S0032-0633(96)00100-6.
Potter, A. E., R. M. Killen, and M. Sarantos (2006), Spatial distribution of sodium on Mercury, *Icarus*, *181*, 1–12, doi:10.1016/j.icarus.2005.10.026.
Raines, J. M., D. J. Gershman, J. A. Slavin, T. H. Zurbuchen, H. Korth, B. J. Anderson, S. C. Solomon (2014), Structure and dynamics of Mercury's magnetospheric cusp: MESSENGER measurements of protons and planetary ions, *J. Geophys. Res. Space Physics*, *119*, 6587–6602, doi:10.1002/2014JA020120.
Richer, E., R. Modolo, C. Chanteur, S. Hess, F. Leblanc (2012), A global hybrid model for Mercury's interaction with the solar wind: Case study of the dipole representation, *J. Geophys. Res.*, *117*, A10228, doi:10.1029/2012JA017898.
Sarantos, M., P. H. Reiff, T. W. Hill, R. M. Killen, and A. L. Urquhart (2001), A Bx-interconnected magnetosphere model for Mercury, *Planet. Space Sci.*, *49*, 1629–1635.
Sarantos, M., R. M. Killen, and D. Kim (2007), Predicting the long-term solar wind ion-puttering source at Mercury, *Planet. Space Sci.*, *55*, 1548–1595, doi:10.1016/j.pss.2006.10.011.
Sarantos, M., J. A. Slavin, M. Benna, S. A. Boardsen, R. M. Killen, D. Schriver, and P. Tràvniček (2009), Sodium-ion pickup observed above the magnetopause during MESSENGER's first Mercury flyby: Constraints on neutral exospheric models, *Geophys. Res. Lett.*, *36*, L04106, doi:10.1029/2008GL036207.
Slavin, J. A., et al. (2010), MESSENGER observations of extreme loading and unloading of Mercury's magnetic tail, *Science*, *329*, 665–668, doi:10.1126/science.1188067.
Slavin, J. A., et al. (2014), MESSENGER observations of Mercury's dayside magnetosphere under extreme solar wind conditions, *J. Geophys. Res. Space Physics*, *119*, 8087–8116, doi:10.1002/2014JA020319.
Sprague, A. L., R. W. H. Kozlowski, D. M. Hunten, N. M. Schneider, D. L. Domingue, W. K. Wells, W. Schmitt, and U. Fink (1997), Distribution and abundance of sodium in Mercury's atmosphere, 1985–1988, *Icarus*, *129*, 2, 506–527, doi:10.1006/icar.1997.5784.
Varela, J., F. Pantellini, and M. Moncuquet (2016), Plasma streams in the Hermean dayside magnetosphere: Solar wind injection through the reconnection region, *Planet. Space Sci.*, *122*, 46–52, doi:10.1016/j.pss.2016.01.008.
Weider, S. Z., et al. (2015), Evidence for geochemical terranes on Mercury: Global mapping of major elements with MESSENGER's X-Ray Spectrometer, *Earth Planet. Sci. Lett.*, *416*, 109–120, doi:10.1016/j.epsl.2015.01.023.
Winslow, R. M., et al. (2014), Mercury's surface magnetic field determined from proton-reflection magnetometry, *Geophys. Res. Lett.*, *41*, 4463–4470, doi:10.1002/2014GL060258.